Supporting Information

Three-Dimensional Continuous Conductive Nanostructure for Highly Sensitive and Stretchable Strain Sensor

Donghwi Cho,[†] *Junyong Park,*[†] *Jin Kim,*[†] *Taehoon Kim,*[†] *Jungmo Kim,*[†] *Inkyu Park,*[‡] *and Seokwoo Jeon*[*,†]

[†]Department of Materials Science and Engineering, KAIST Institute for The Nanocentury, Korea Advanced Institute of Science and Technology (KAIST), Daejeon 34141, Republic of Korea

[‡]Department of Mechanical Engineering, KAIST Institute for the Nanocentury, Korea Advanced Institute of Science and Technology (KAIST), Daejeon 34141, Republic of Korea

[*]Correspondence should be addressed to S.J. (email: jeon39@kaist.ac.kr)

Supporting Figures and Captions

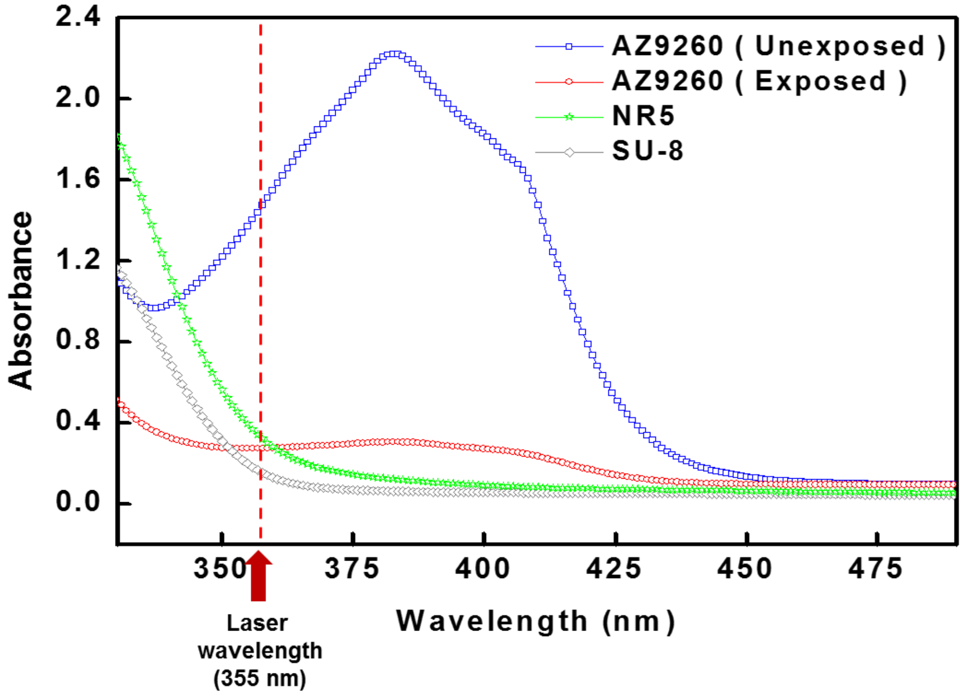

Figure S1. Optical absorption of the previously used photoresists for PnP induced by photo exposure. (Blue open squares: unexposed AZ 9260 (Clariant), red open circles: exposed AZ 9260, green stars: NR5 (Futurrex), grey rhombi: SU-8 (Microchem).

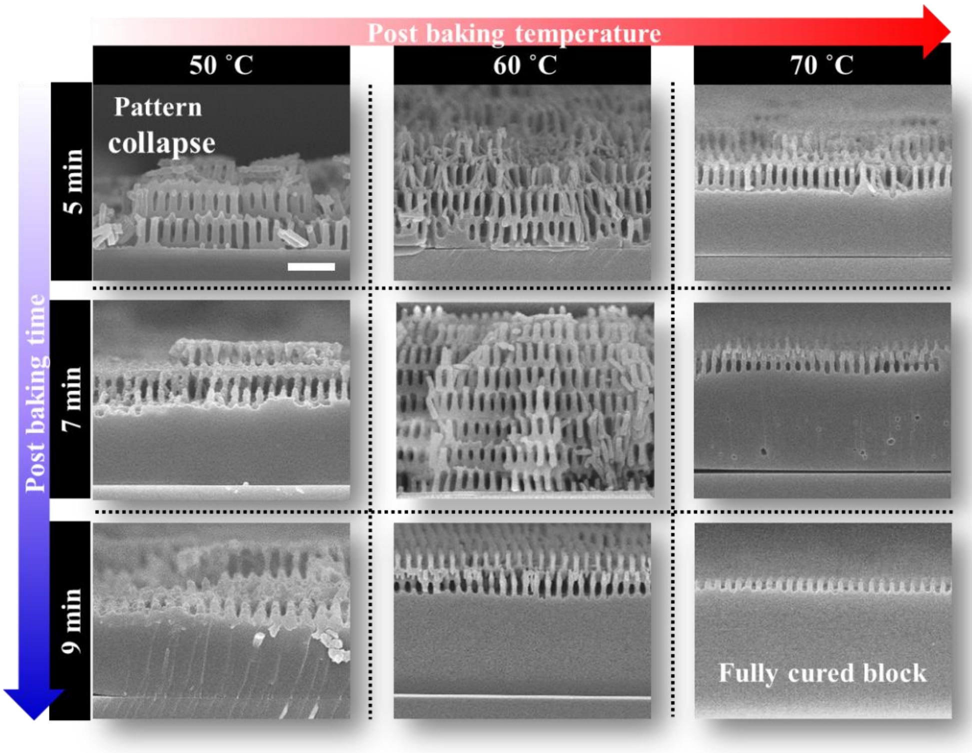

Figure S2. Cross-sectional SEM images of the 3D nanostructure with varying post baking time and temperature. Overheating can make the 3D porous structure blocked. On the other hand, not enough heat can make the pattern collapse (scale bar, 2μm).

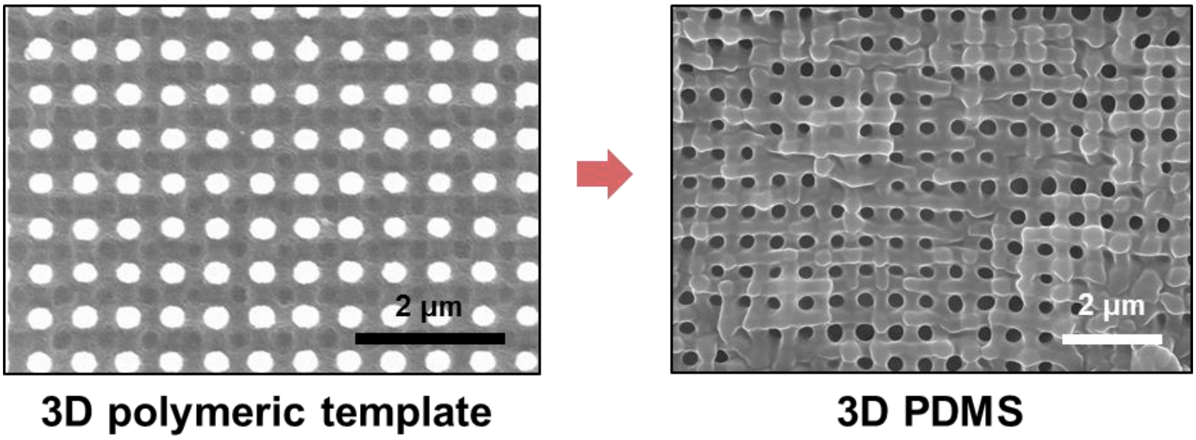

Figure S3. Top view SEM images of the 3D polymeric template defined by PnP and the 3D PDMS.

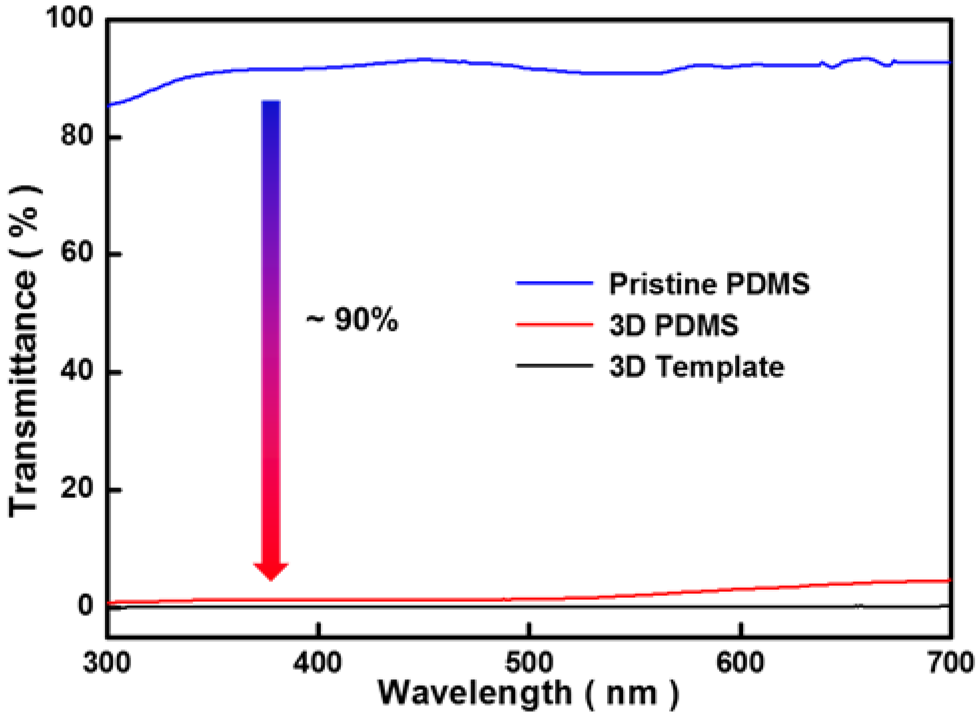

Figure S4. Transmittance spectra comparison of 3D polymer template defined by PnP, 3D PDMS, and pristine PDMS.

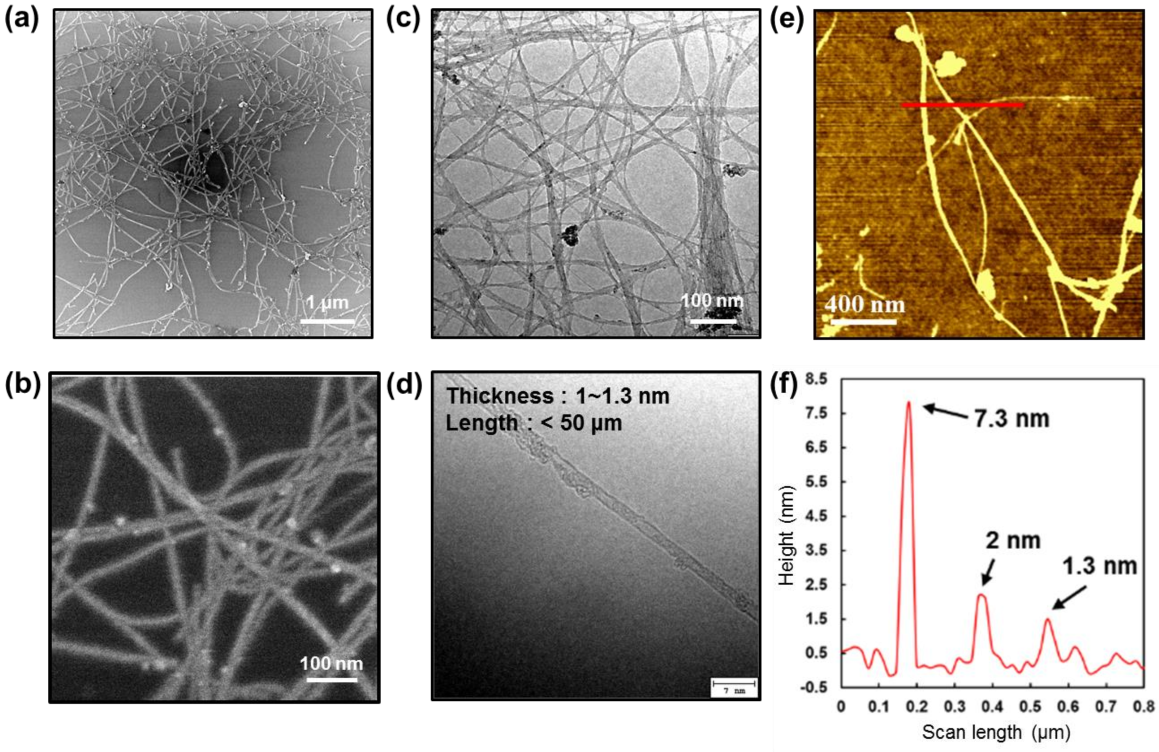

Figure S5. Characterization of SWCNTs used for conductive filler in 3D continuous conductive nanostructure. **(a)** A top view SEM image. **(b)** A magnified top view SEM image. **(c)** A TEM image. **(d)** A magnified view TEM image. **(e,f)** An AFM topography image and corresponding height profile.

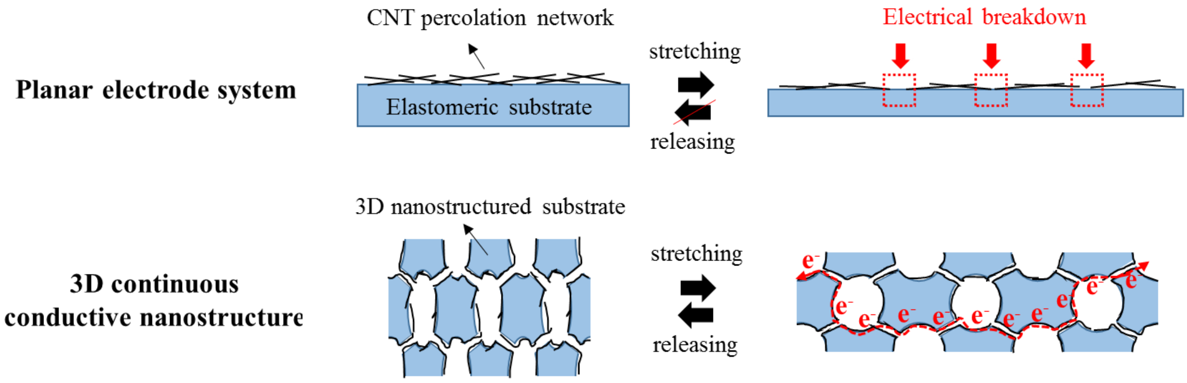

Figure S6. Schematics for a conductive percolation network in thin-film based planar electrode system and the 3D bicontinuous nanoporous electrode during the stretching and releasing process.

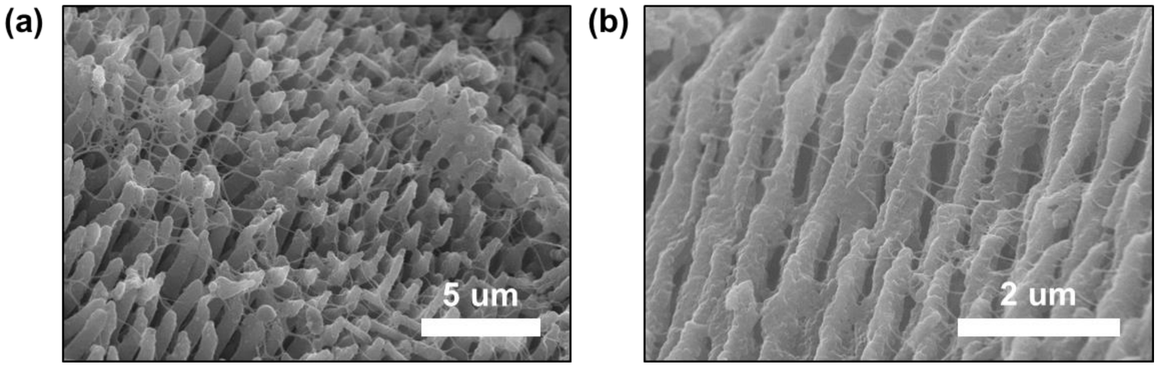

Figure S7. Infiltration of SWCNT solution into 3D polymer template which has a hydrophobic nature. **(a)** Tilted-view of top SEM image. **(b)** Cross-sectional view SEM image.

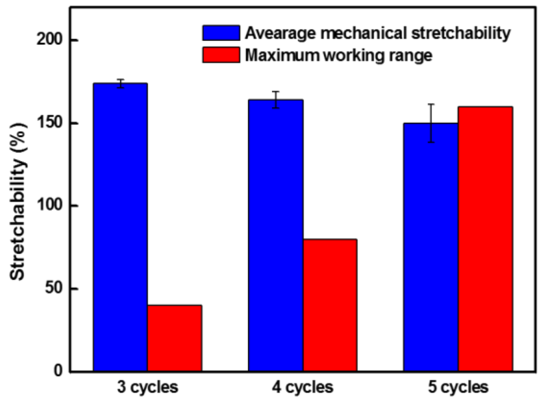

Figure S8. Comparison of the average mechanical stretchability based on stress-strain curves and the maximum working ranges of the samples with different infiltrating cycles.

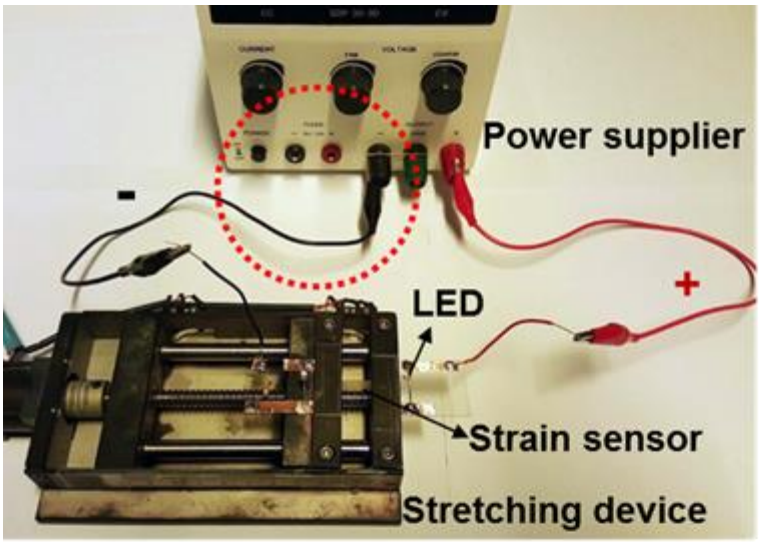

Figure S9. Optical image of the LED set-up integrated with the 3D strain sensor on the stretching tester. Integrating two LEDs, each positioned at opposite ends, the 3D continuous conductive nanostructure is uniaxially stretched along the stretching direction at low strain rates (~2 mm/sec).

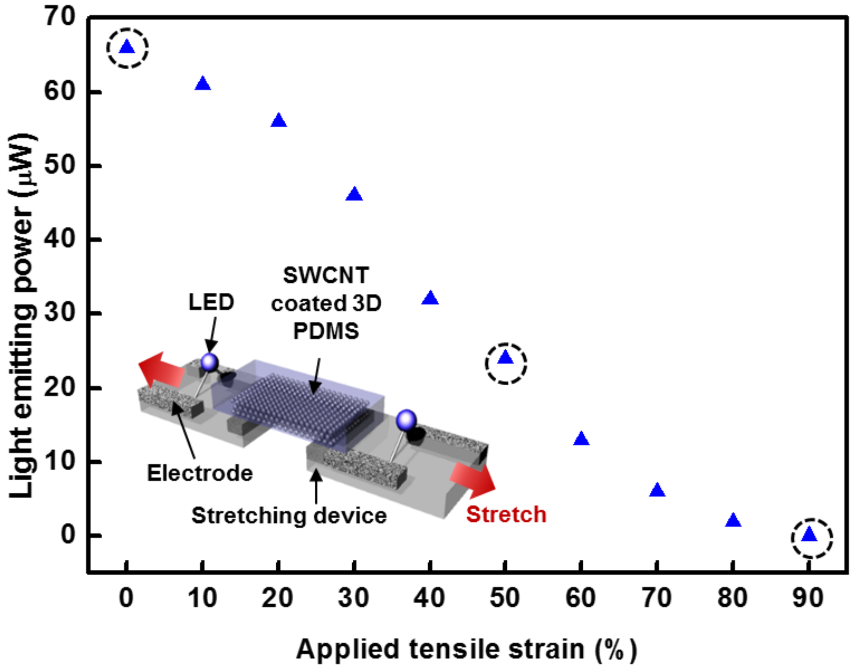

Figure S10. Relationship between applied tensile strain and LED output. Schematic showing the LED set-up with stretching device.

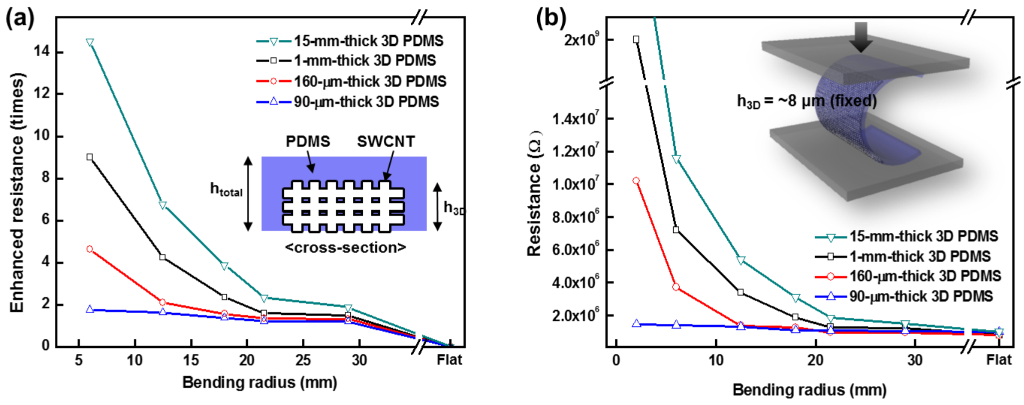

Figure S11. Resistance change of the 3D continuous conductive nanostructure under various bending radii. **(a)** Resistance increase compared to initial resistance with different total thickness of the 3D PDMS under bending state. **(b)** Response curves when the sensor is bent to various bending radii for different total thicknesses with varying backing layer thickness.

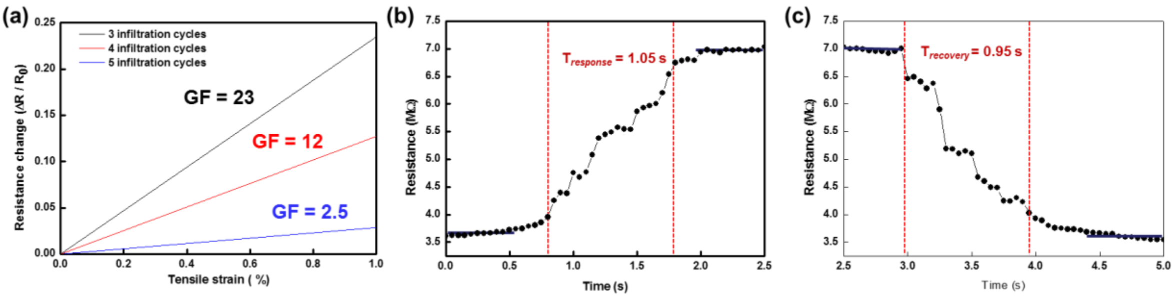

Figure S12. Electromechanical properties of the 3D strain sensor. **(a)** Resistance variation versus strain within strain range of 0-1%. **(b,c)** The response and recovery time evaluation by time-resolved detection of resistance change.

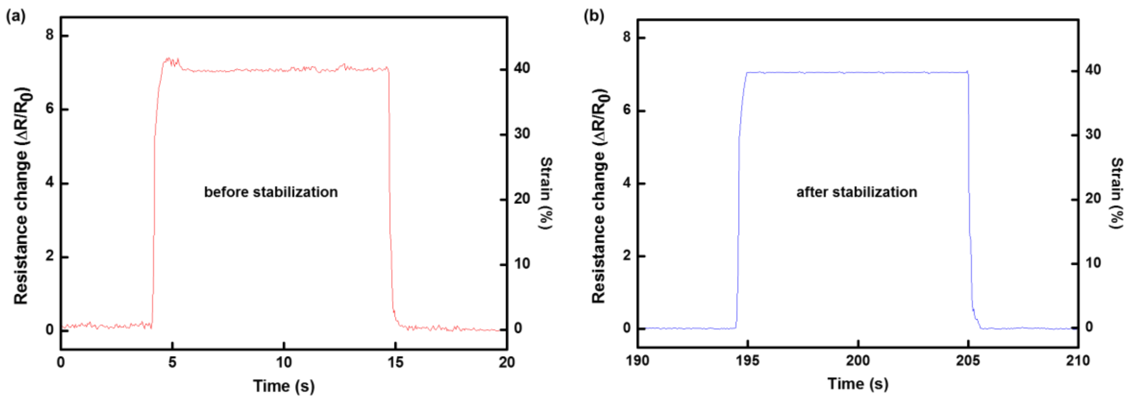

Figure S13. The resistance change of the 3D strain sensor with 4 infiltration cycles for the first 10 repetitive 40 % stretching and releasing cycles in Figure 4e. **(a)** The close-up of the region of the red box in Figure 4e. **(b)** The close-up of the region of the blue box in Figure 4e.

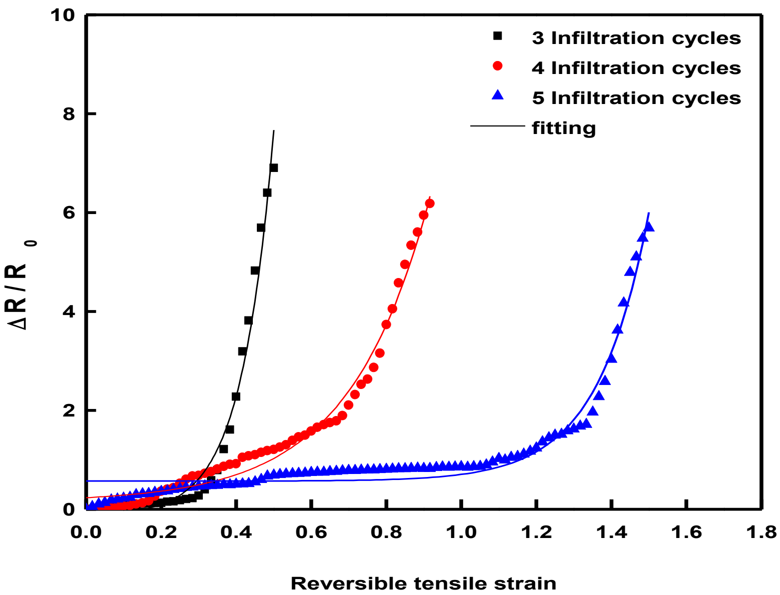

Figure S14. Resistance change of the 3D strain sensor infilled with PDMS as an index-matching material. Strain dependent $\Delta R/R_0$ of the sensors at each stretching strain ranging from 0% to 50%, to 90%, to 150%, respectively.